Bergische Universität Wuppertal

Fakultät für Mathematik und Naturwissenschaften

Institute of Mathematical Modelling, Analysis and Computational Mathematics (IMACM)

Preprint BUW-IMACM 21/37

Sergey Pereselkov, Venedikt Kuz'kin, Matthias Ehrhardt and Kaznacheev Ilya

# Experimental observation and analysis of the low-frequency source interference pattern

December 20, 2021

http://www.imacm.uni-wuppertal.de

Article

# Experimental observation and analysis of the low-frequency source interference pattern

**Sergey Pereselkov [1,*], Venedikt Kuz'kin [2,], Matthias Ehrhardt [3,] and Kaznacheev Ilya [1,]**

[1] Voronezh State University, Russia; pereselkov@yandex.ru
[2] Prokhorov General Physics Institute of the Russian Academy of Sciences, Russia; kumiov@yandex.ru
[3] University of Wuppertal, Gaußstraße 20, 42119 Wuppertal, Germany; ehrhardt@uni-wuppertal.de
* Correspondence: e-mail@e-mail.com;

**Abstract:** The sound field interference pattern of broadband source in shallow water waveguide was studied experimentally. The acoustic experiment was carried out on the Pacific shelf in 2004. The acoustic signals were emitted by the airgun source (with frequency band 5–200 Hz). The source was towed with speed 1.7 m/s at depth 15 m along different paths. Several bottom receivers were used for recording acoustics signals. The experimental records are processed to obtain sound intensity distributions (interferograms) $I(\omega, t)$ in frequency-time domain for different paths of source motion. The two-dimensional Fourier transform (2D-FT) is applied to analyze the experimental interferograms. The result of the 2D-FT $F(\nu, \tau)$ can be called the Fourier-hologram (hologram). The hologram allows us to coherently accumulate the sound intensity of interferogram in the narrow area as focal spots. It is demonstrated in the paper that position of focal spots in the experimental hologram depends on radial speed of the source, motion direction of the source and the distance between the source and the receiver. As a result, the position of focal spots can be used for estimation of the source parameters.

**Keywords:** sound field; waveguide; interference pattern; hologram; source detection; vector sensor; signal processing

**Citation:** Pereselkov, S.; Kuz'kin, V.; Ehrhardt, M.; Kaznacheev, I. Title. *Journal Not Specified* **2022**, *1*, 0. https://doi.org/

Received:
Accepted:
Published:



## 1. Introduction

The normal-mode interference of sound field in underwater waveguide leads to structured pattern that can be observed in sound intensity distribution in the frequency-time domain (Weston and Stevens[1]) or frequency-range domain (Chuprov [2]). The sound field interference theory in underwater acoustics was offered by Chuprov [2]. He offered the conception of the waveguide invariant - basic parameter of sound field interference pattern. The more significant achievements in the interference theory are presented in the following papers: Grachev[3], Orlov and Sharonov[4] and papers of Conf. Proc. ed. by Kuperman and D'Spain[5].

The developed interference theory in ocean waveguide allowed to solve a set of important problems of underwater acoustics: source localization (passive mode[6–9] and active mode[10]), remote sensing of geo-acoustic parameters[11], effective signal processing[12,13].

One of the important advancements of the interference theory is the approach to the analysis of the interference pattern proposed in papers: Rouseff and Spinde [15], Baggeroer[14], and Yang[16]. Within the framework of this approach the interference pattern is considered as sound intensity distributions $I(\omega, r)$ in frequency-range domain or $I(\omega, t)$ in frequency-time domain. The two-dimensional Fourier transform (2D-FT) of $I(\omega, r)$ is applied to analyze sound intensity distributions. At first, this approach allows to estimate waveguide invariant[15]. The estimation of waveguide invariant is the extremum of the "reference" distribution of 2D-FT. Secondly, this approach allows to coherently accumulate the sound intensity of interferogram in the narrow area as focal spots and rise the signal-noise ratio (SNR) significantly[8,9].

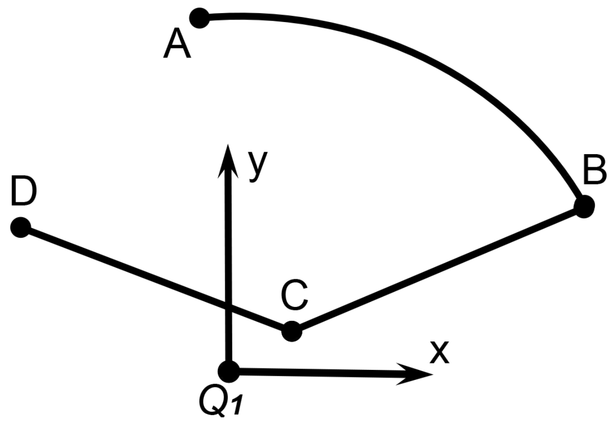


**Figure 1.** The experiment scheme. Top view.

The purpose of this paper is to present experimental observation of the interference pattern and results of analysis by 2D-FT. The experimental records are processed to obtain sound intensity distributions (interferograms) $I(\omega, t)$ in the frequency-time domain for different paths of source motion. The two-dimensional Fourier Transformation (2D-FT) is applied to analyze the experimental interferograms. The result of the 2D-FT $F(\nu, \tau)$ can be called the Fourier-hologram (hologram). The hologram allows us to coherently accumulate the sound intensity of interferogram in the narrow area as focal spots.

This paper consists of the three sections. The Pacific shelf experiment is described in the Sec. II. The theory of interferogram and hologram of moving source is presented in the Sec. III. The experimental results of interferograms and holograms are considered for different paths of source motion in the Sec. IV. It is demonstrated in the paper that the position of focal spots in the experimental hologram depends upon radial speed of source, motion direction and distance from a receiver. As a result, the displacement of focal spots in hologram domain can be used for estimation of source parameters mentioned above.

## 2. Experiment

The acoustics experiment was carried out on the Pacific shelf (Yellow Sea) in 2004. The water depth was a $H \approx 53$ m. The sound speed in water layer $c \approx 1474$ m/s. These acoustic parameters were approximately constant in experimental region. The airgun was used as broadband sound source. The sound source was towed by research vessel. The source depth was $z_s \approx 15$ m. The towing velocity was $v \approx 1.7$ m/s. The airgun had a pulse signature that was found to be quite repeatable. The signal pulses were controlled by monitor hydrophone located at distance of 2 m from the source. The airgun produced broadband pulses that had consistently repeatable spectra in the band $\Delta f \approx 10 - 250$ Hz. The pulses were separated with time interval $T = 30$ s. During the experiment, the signals of airgun source were received by stationary vector-scalar receivers (VSR), which had channels for measuring pressure and vibration velocity three components. The pressure measurement results from the VSR located at a depth $z_q \approx 52$ m are used for signal processing presented in the paper. The received signals are analyzed in the band $\Delta f \approx 80 - 120$ Hz. The amplitude of airgun pulses was normalized to the same value in order to keep constant the interference-pattern contrast.

The motion geometry of the towed airgun source and the position of VSR $Q_1$ are shown in Fig. 1. The source moved along an arc of radius $r_0 \approx 11$ km from the initial point $A$ to the point $B$. Point $A$ was located approximately in the direction of the $y$ axis of VSR $Q_1$. At point $B$, the source motion was turned to the strait one. After point $B$ the source approached the VSR $Q_1$ along straight-line path from point $B$ to point $C$. The point $C$ was located near the receiver VSR $Q_1$. The distance between point $C$ and the x axis was

$r_C \approx 1$ km. At point $C$ the source was turned and moved along a straight-line path away from VSR $Q_1$ to point $D$.

## 3. The sound field interference pattern of the moving source

Let us consider ocean waveguide as a water layer bounded in depth by free surface and bottom. We use the model of a uniform continuous spectrum of a source. We present the sound field intensity of the source as a superposition of the modes as the following:

$$I(\omega, r) = \sum_m \sum_n A_m(\omega, r) A_m^*(\omega) \exp[irh_{mn}(\omega)] \tag{1}$$

where $h_{mn}(\omega) = h_m(\omega) - h_n(\omega)$. Here $A_m(\omega, r)$ is mode amplitude, $h_m(\omega)$ is horizontal wavenumber of the $m$-th mode, $\omega = 2\pi f$ is the cyclical frequency of the source spectrum, and $r$ is the distance between the source and receiver. The cylindrical divergence of the sound field and the mode attenuation are taken into account by the distance dependence of the mode amplitudes. The constant factor determining the source spectrum value is omitted in front of the sum. This factor is inessential for the following analysis. The right-hand part of Eq. (1), can be rewritten as the double sum of the terms corresponding to the interference of a modes pair :

$$I(\omega, r) = \sum_m \sum_n I_{mn}(\omega, r) \tag{2}$$

where

$$I_{mn}(\omega, r) = A_m(\omega, r) A_n^*(\omega, r) \exp[irh_{mn}(\omega)] \tag{3}$$

We assume, that the number of modes is equal to $M$, and the number of the first mode is $m = 1$.

Let us consider the signal spectrum in the frequency band $-\Delta\omega/2 + \omega_0 \leq \omega \leq \omega_0 + \Delta\omega/2$ and in the time interval $t_0 \leq t \leq t_0 + \Delta t$. The source-receiver distance increment is $\Delta r$ within the observation time $\Delta t$. The initial source-receiver distance is $r_0$ at the initial time $t_0$. In the case of the constant source velocity we can represent the source-receiver distance increment in the following form:

$$\Delta r = v_r \Delta t \left( \cos\varphi + v_r \Delta t \sin^2\varphi / 2r_0 \right) \tag{4}$$

where $\varphi$ is the angle between the source-receiver direction and the source motion direction, $v_r$ is the radial velocity value. In the Eq. (4) the quadratic term is ignored under condition $\Delta t \ll 2r_0 \cos\varphi / v_r sin^2\varphi$. This condition imposes a restriction for the duration of observation depending on the velocity, the initial distance, and the angle of trajectory.

Let us put the right side of Eq. (4) in expressions Eq. (1)–Eq. (3). As a result, we pass from variable $r$ in $I(\omega, r)$ to variable $t$ in $I(\omega, t)$. Then we apply two-dimensional Fourier transform (2D-FT) for interferogram $I(\omega, t)$ (Eq. (2)) in the frequency–time variables $(\omega, t)$

$$F(\tilde{v}, \tau) = \sum_m \sum_n F_{mn}(\tilde{v}, \tau). \tag{5}$$

where $\tilde{v} = 2\pi\nu$ is the cyclical frequency of the hologram domain, $\tau$ is time of the hologram domain.

Let us analyze the term in the right side of Eq. (5):

$$F_{mn}(\tilde{v}, \tau) = \int\limits_0^{\Delta t} \int\limits_{\omega_0 - \frac{\Delta\omega}{2}}^{\omega_0 + \frac{\Delta\omega}{2}} I_{mn}(\omega, t) \exp[i(\tilde{v}t - \omega\tau)] dt d\omega. \tag{6}$$

We use linear approximation of horizontal wavenumber $h_m(\omega)$ as the following function of frequency:

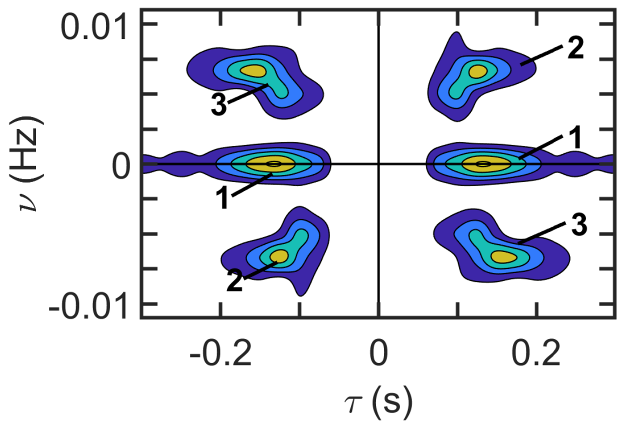


**Figure 2.** The modeling results of Fourier-hologram for different paths of source movement (4 m/s): 1 – source moves along arc between A and B; 2 – source moves from B to C; 3 – from C to D.

$$h_m(\omega) = h_m(\omega_0) + \frac{dh_m(\omega_0)}{d\omega}(\omega - \omega_0) \tag{7}$$

Then, we assume that modes with numbers close to the $l$-th mode interfere constructively. By considering the number of mode as a continuous variable, we can obtain

$$\begin{aligned} F_{mn}(\tilde{\nu}, \tau) = A_m A_n^* \exp\left[ i\left( \frac{\tilde{\nu}\Delta t}{2} - \tau\omega_0 \right) \right] \Delta\omega\Delta t \\ \times \exp\left\{ i\left[ (m-n)\alpha\left( \frac{\Delta t}{2} v_r + r_0 \right) + r_0(\tilde{\nu}/v_r) \right] \right\} \\ \times \frac{\sin\left\{ \left[ (r_0 + v_r t_{mn})(m-n)\frac{d\alpha}{d\omega} - \tau \right] \frac{\Delta\omega}{2} \right\}}{\left[ (r_0 + v_r t_{mn})(m-n)\frac{d\alpha}{d\omega} - \tau \right] \frac{\Delta\omega}{2}} \\ \times \frac{\sin\left\{ [v_r(m-n)\alpha + \tilde{\nu}] \frac{\Delta t}{2} \right\}}{[v_r(m-n)\alpha + \tilde{\nu}] \frac{\Delta t}{2}} \end{aligned} \tag{8}$$

where $\alpha = dh_l(\omega_0)/dl$. The introduction of expansion Eq. (7) proves useful for interpreting the hologram structure. In reality, according to Eq. (7) $(d\alpha/d\omega)(m-n) = dh_{mn}(\omega_0)/d\omega$, $\alpha(m-n) = h_{mn}(\omega_0)$. Here $d\omega/dh_m = u_m$, is the group velocity of the $m$-th mode.

Hologram Eq. (5) is localized in two domains symmetrically located with respect to the origin of the plane $(\tilde{\nu}, \tau)$. This feature of the hologram is the result of the function symmetry (Eq. (8)): $F_{mn}(\tilde{\nu}, \tau) = F_{nm}(-\tilde{\nu}, -\tau)$. The hologram is located on on the $\tau$-axis of plane $(\tilde{\nu}, \tau)$ if the radial velocity $v_r = 0$ i.e., the source - receiver distance is constant (Fig. 2, peak – 1). The hologram is located in quadrants II and IV of plane $(\tilde{\nu}, \tau)$ if the radial velocity $v_r > 0$ if the angle of the trajectory $0 \leq \varphi < \pi/2$ (Fig. 2, peak – 2). The hologram is located in quadrants I and III of plane $(\tilde{\nu}, \tau)$ if the radial velocity $v_r < 0$ i.e., the angle of the trajectory $\pi/2 < \varphi \leq \pi$ (Fig. 2, peak – 3). As a result, it is possible to estimate by the hologram if the source is moving away from receiver or to receiver.

Let us estimate the main maxima positions of hologram as follows

$$\begin{aligned} \tau_{mn} &= (r_0 + v_r t_{mn})(m-n)\frac{d\alpha}{d\omega}, \\ \tilde{\nu}_{mn} &= -v_r(m-n)\alpha. \end{aligned} \tag{9}$$

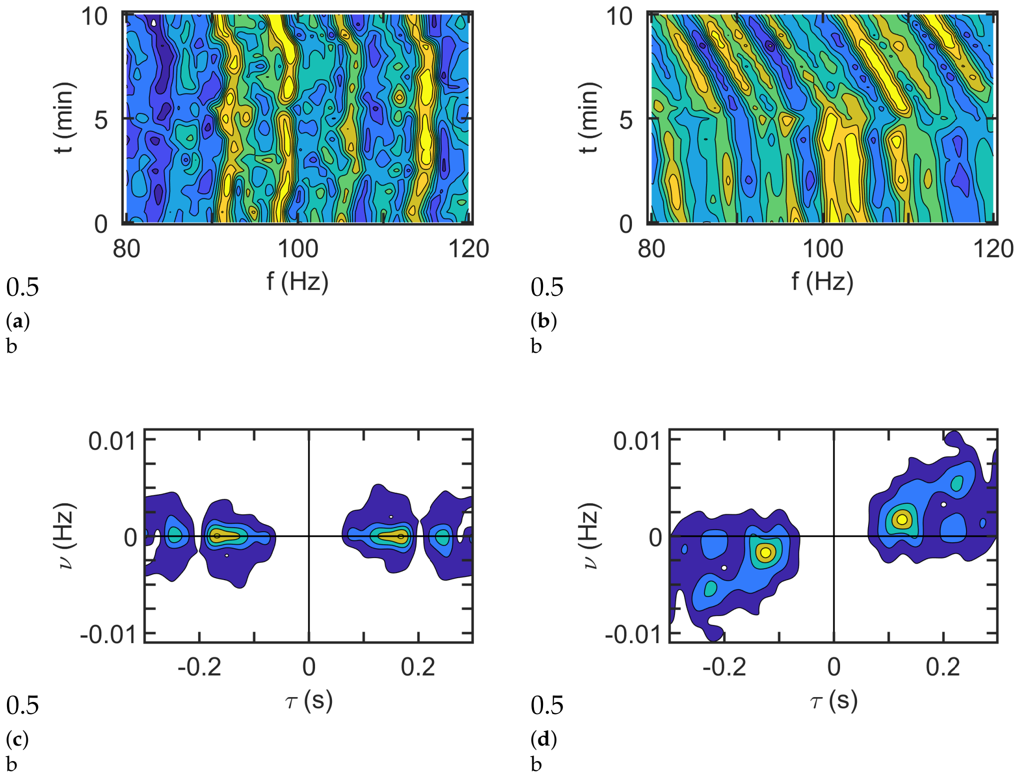


**Figure 3.** The experimental normalized interferograms (a,b), holograms (c, d): (a,c) - the source motion along the arc between A and B; (b,d) - the source motion turn around B.

Thus, the positions of the focal spots maxima in the hologram are proportional to the radial velocity $v_r$ and to the initial distance between the source and the receiver ($r_0$).

The values $t_{mn}$ are constricted to a small vicinity of some point $t_1$ in the observation interval $\Delta t$ ($0 < t_1 < \Delta t$) and it is possible to set $t_{mn} \approx t_1$. Here, qualitatively and quantitatively, as seen below, the results remain quite reasonable.

## 4. Experimental Results

The results of experimental data processing are shown in Fig. 3 and Fig. 4. The dynamics of normalized values of interferogram Eq. (1) and hologram Eq. (7) for received signals are shown for different types of the source motion.

The interferogram in Fig. 3 (a) and the hologram in Fig. 3 (c) correspond to the movement of the source along the arc of radius $r_0 \approx 11\,km$ between point $A$ and point $B$. One can see that interference bands are different from vertical lines. This implies that the source path differs from the arc of a circle. At the same time, the position of the main hologram peaks on the time axis (Fig. 3 (c)) indicates that the source radial velocity is zero. The presence of two peaks in the hologram (Fig. 3 (c)) indicates that the field is formed by three modes. It should be noted that the interferogram and hologram are identical for an immobile source and for the source moving along arc. Value of arc radius $r_0$ can be estimated from the formula Eq. (9) on the assumption that the radial velocity $v_r = 0$. Then, we obtain the following expression:

$$r_0 = \frac{2\tau_1}{1/u_3 - 1/u_1} \tag{10}$$

where $u_i$ is the group velocity of the $i$-th mode. As follows from Fig. 3 (c), $\tau_1 = 0.168$ s. Under the experimental conditions at the reference frequency $f_0 = 100$ Hz, the group

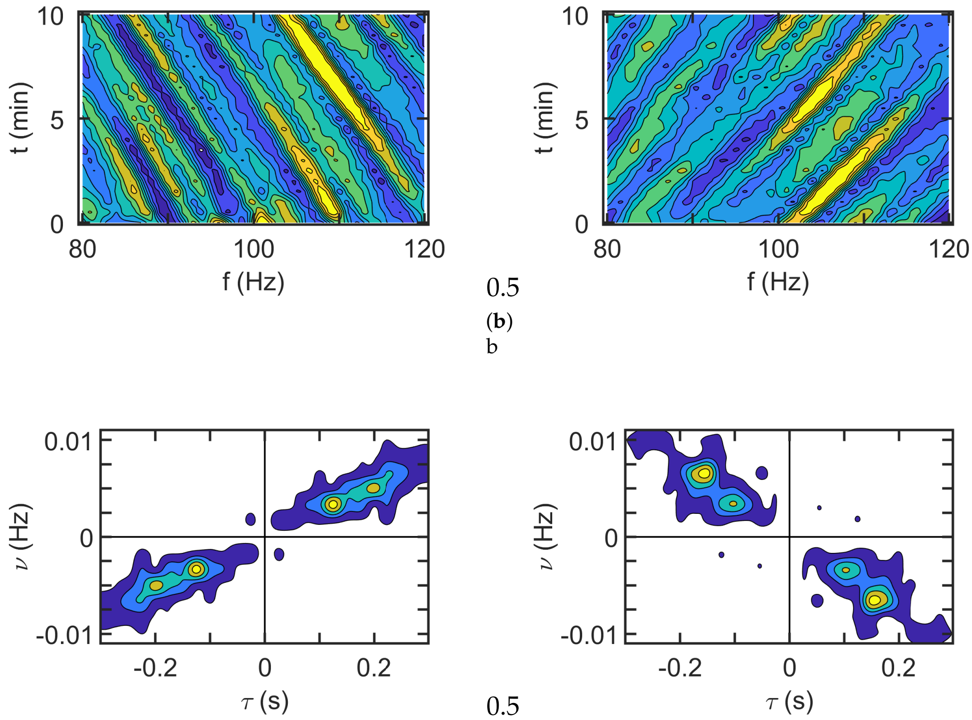


0.5 **(a)** b 0.5 **(b)** b 0.5 **(c)** b 0.5 **(d)** b

**Figure 4.** The experimental normalized interferograms (a,b), holograms (c, d): (a,c) - the source motion between B and C; (b,d) - the source motion between C and D.

velocities $u_1$ and $u_3$ are, respectively, 1462.8 m/s and 1399.5 m/s. As a result, we obtain $r_0 = 10.9$ km.

The sound field interference pattern at the point B of the motion path along the arc of a circle passes to a straight line towards the VSR $Q_1$ is shown in Fig. 3 (b). The break in the band is observed in the interferogram (Fig. 3 (b)) at $t_i \approx 5$ min, which corresponds to the source rotation near point B (see Fig. 1). The form of the hologram (Fig. 3 (d)) shows that the source radial velocity turn is nonzero during the rotation. The coordinates of the main peak in the hologram are $\tau_1 = 0.139$ s and $\nu_1 = 0.00186$ Hz.

Under the experimental conditions at the frequency $f_0 = 100$ Hz, the propagation constants are $h_1 = 0.4245\ \mathrm{m}^{-1}$ and $h_3 = 0.3995\ \mathrm{m}^{-1}$ and the interference invariant is $\beta = 1.2$. On the assumption that the interference peak frequency corresponding to the instant $t_i \approx 5$ min is $f_1 = 110$ Hz (see Fig. 5(a)), we find that the radial velocity of the source and its distance to the VSR $Q_1$ at the rotation point B are, respectively, $v_r = -0.92$ m/s and $r = 10.8$ km.

The sound field interferogram and hologram for a source moving from point B to point C (to VSR $Q_1$) are shown in Fig. 4 (a) and (c).

The sound field interferogram and hologram for a source moving from point C to point D (away from VSR $Q_1$) are shown in Fig. 4 (b) and (d).

The interference patterns (Fig. 4 (a),(c)) are sets of straight-line localized bands. It indicates that source motion direction and radial velocity are constant.

The bands slopes have opposite signs for different source direction. As compared with the case of a source moving along the arc from A to B, the holograms have more main peaks. That indicates the increasing the number of sound field modes. For a source motion to VSR $Q_1$, the main-peak coordinates are $\tau_1 = 0.145$ s and $\nu_1 = 0.0032$ Hz (Fig. 4 (b)). For a source motion from the VSR $Q_1$. $\tau_1 = 0.127$ s, $\nu_1 = 0.0035$ Hz (Fig. 4 (d)), As a result, we have the following estimates of the radial velocity and the distance to the source: $v_r = -1.67$ m/s and $r = 9.7\,\mathrm{km}$ for the case of source motion to VSR $Q_1$ and $v_r = 1.88\,\mathrm{m/s}$ and $r = 8.3\,\mathrm{km}$ for the case of source motion from away the VSR $Q_1$. As one would expect, the slope ratio for the straight lines which contain the main peaks of the hologram is equal to the ratio of source radial velocities:

$$\gamma = -\frac{0.0315}{0.025} = -\frac{1.88}{1.67} = -1.26\,.$$

Fig. 3 (d) shows how the focal spots become diffuse when the path shape changes. The focal spot size is minimum when a source moves along a circular or straight-line path Fig. 3 (c) and Fig. 4 (c),(d). when the interference band slope is constant.

At the same time, the peaks localization region is expanded at the point where the path changes from an arc of a circle to a straight line (Fig. 3 (d)).

## 5. Conclusions

The results of the analysis of sound field interfer- ence pattern of a broadband source in shallow water are presented in the paper. The experimental records are processed to obtain interferogram for different paths of source motion. The Fourier-hologram is used to analyze the experimental interferograms. It is shown in the paper that the hologram allows us to coherently accumulate the sound intensity of interferogram in the narrow area as fo- cal peaks along the line, passing through the origin. It is demonstrated in the paper that position of focal spots in experimental hologram depends upon radial speed of source, movement direction and distance from receiver. The position of the main hologram peaks are on the time axis in the case of the source movement along the arc. It means that source radial velocity is zero. The hologram peaks are located in quadrants I and III when the source moves towards the receiver. In the case of the source movement away from the receiver, the hologram peaks are in quadrants II and IV . Estimations of source parameters are presented for different directions of source movement in the experiment. Good consistency of the experimental and estimated values demonstrates the ef- ficiency of this approach for solving source localization problems. Thus, it is possible to use interferograms and holograms as a potential basis for applying holographic interferometry in the passive location of the source. This approach allows to solve complex problem of detecting a source and estimating its velocity, distance and depth by using only a single receiver.

**Author Contributions:** For research articles with several authors, a short paragraph specifying their individual contributions must be provided. The following statements should be used "Conceptualization, X.X. and Y.Y.; methodology, X.X.; software, X.X.; validation, X.X., Y.Y. and Z.Z.; formal analysis, X.X.; investigation, X.X.; resources, X.X.; data curation, X.X.; writing—original draft preparation, X.X.; writing—review and editing, X.X.; visualization, X.X.; supervision, X.X.; project administration, X.X.; funding acquisition, Y.Y. All authors have read and agreed to the published version of the manuscript.", please turn to the CRediT taxonomy for the term explanation. Authorship must be limited to those who have contributed substantially to the work reported.

**Funding:** Please add: "This research received no external funding" or "This research was funded by NAME OF FUNDER grant number XXX." and and "The APC was funded by XXX". Check carefully that the details given are accurate and use the standard spelling of funding agency names at https://search.crossref.org/funding, any errors may affect your future funding.

## References

1. Weston, D. E., and Stevens, K. J. (**1972**). "Interference of wide band sound in shallow water," J. Sound. Vib. **21**(1), 57–64.
2. Chuprov, S. D. (**1982**). "Interference structure of a sound field in a layered ocean," in *Ocean Acoustics Current State*, (Nauka), pp. 71–91.
3. Grachev, G. A. (**1993**). "Theory of acoustic field invariants in layered waveguides,", Acoust. Phys. **39**(1), 67–71.
4. Orlov, E. F., and Sharonov, G. A. (**1998**). "Interference of sound waves in the ocean,", (Dal'nauka).
5. Kuperman, W. A. and D'Spain, G. L. (**2002**). "Ocean Acoustic Interference Phenomena and Signal Processing. AIP Conf. Proc. ed. by W. A. Kuperman and G. L. D'Spain," **621**, (AIP, Melville, NY).
6. Thode, A. M. (**2000**). "Source ranging with minimal environmental information using a virtual receiver and waveguide invariant theory," The Journal of the Acoustical Society of America **108**(4), 1582–1594.

7. Cockrell, K. L., and Schmidt, H. (**2010**). “Robust passive range estimation using the waveguide invariant,” The Journal of the Acoustical Society of America **127**(5), 2780–2789.
8. Kuz’kin, V. M., Pereselkov, S. A., Kuznetsov, G. N., and Kaznachheev, I. V., (**2017**). “Noise source localization shallow water,” Phys. Wave Phenom. **25**(2), 156–163.
9. Kuz’kin, V. M., Pereselkov, S. A., Kuznetsov, G. N., and Kaznachheev, I. V., (**2018**). “An Interferometric Method for Detecting a Moving Sound Source with a Vector-Scalar Receiver,” Acoustical Physics **64**(1), 37–48.
10. Quijanoa, J. E., Zurkb, L. M., and Rouseff, D. (**2008**). “Demonstration of the invariance principle for active sonar,” The Journal of the Acoustical Society of America **123**(3), 1329–1337.
11. Heaney, K. D. (**2004**). “Rapid geoacoustic characterization using a surface ship of opportunity,” IEEE J. Ocean. Eng. **29**(1), 88–99.
12. Bonnel, J., Touze, G. Le., and Mars, J. I. Bonnel, J. (**2013**). “Physics-based timefrequency representations for underwater acoustics: Power class utilization with waveguide invariant approximation,” IEEE Signal Process. Mag. **30**(6), 120–129.
13. Gall, Y. Le., and Bonnel, J. (**2013**). “Separation of moving ship striation patterns using physics-based filtering,” Traitement du Signal **30**(3-5), 149–168.
14. Baggeroer, A. B. (**2002**). “Estimation of the distribution of the interference invariant with seismic streamers,” AIP Conf. Proc. **621**, 151–170.
15. Rouseff, D., and Spindel, R. C. (**2002**). “Modeling the waveguide invariant as a distribution,” AIP Conf. Proc. **621**, 137–150.
16. Yang, T. C., (**2003**). “Beam intensity striations and applications,” The Journal of the Acoustical Society of America **113**(3), 1342–1352.